ENVIRONMENTAL RESEARCH
LETTERS

LETTER

Heatwave reveals potential for enhanced aerosol formation in Siberian boreal forest

Olga Garmash[1,2,4,5,*], **Ekaterina Ezhova**[1,5,*], **Mikhail Arshinov**[3], **Boris Belan**[3], **Anastasiia Lampilahti**[1], **Denis Davydov**[3], **Meri Räty**[1], **Diego Aliaga**[1], **Rima Baalbaki**[1], **Tommy Chan**[1], **Federico Bianchi**[1], **Veli-Matti Kerminen**[1], **Tuukka Petäjä**[1] and **Markku Kulmala**[1]

[1] Institute for Atmospheric and Earth System Research/Physics, Faculty of Science, University of Helsinki, Helsinki, Finland
[2] Aerosol Physics Laboratory, Physics Unit, Tampere University, Tampere, Finland
[3] V.E. Zuev Institute of Atmospheric Optics of Siberian Branch of the Russian Academy of Sciences, Tomsk, Russia
[4] Present address: Department of Atmospheric Sciences, University of Washington, Seattle, WA, United States of America.
[5] These authors contributed equally to this work.
[*] Authors to whom any correspondence should be addressed.

E-mail: olga.garmash@helsinki.fi and ekaterina.ezhova@helsinki.fi

Keywords: secondary aerosol, boreal forest, atmospheric chemistry, pollution, BVOC

Supplementary material for this article is available online

OPEN ACCESS

RECEIVED
17 August 2023

REVISED
8 November 2023

ACCEPTED FOR PUBLICATION
29 November 2023

PUBLISHED
9 January 2024

Abstract

Siberia is covered by 6 million km^2 of forest, which moderates climate as a carbon sink and a source of aerosol particles causing negative radiative effect. Aerosol particles in boreal forests frequently form via gas-to-particle conversion, known as new particle formation (NPF). Compared to boreal sites at similar latitudes, NPF was reported to occur less often in the Siberian forest. However, factors controlling NPF in Siberia remain unknown. Our results suggest that the combination of biogenic and anthropogenic contributions caused unexpectedly high monthly NPF frequency (50%) at the observatory Fonovaya in the West Siberian taiga during the Siberian 2020 heatwave. High frequency was due to early spring photosynthetic recovery, which boosted biogenic emissions into polluted air masses carrying SO_2. After mid-April, high temperatures and cleaner air masses led to less frequent (15%) and less intense NPF despite the increased emissions of natural organic vapors and ammonia. Furthermore, the contrast between the two spring periods was seen in cluster composition, particle-forming vapors (two times difference in sulfuric acid concentration), particle formation (J_3, 2.2 and 0.4 cm^{-3} s^{-1}) and growth rates (GR_{2-3}, 1.7 and 0.6 nm h^{-1}). Given the strong warming trend, our results suggest that within 25−30 years, the monthly NPF frequency during early spring in the West Siberian taiga can reach 40%–60%, as in the European boreal sites.

1. Introduction

The boreal forest is a well-known source of atmospheric aerosol particles [1, 2], especially in terms of the particle number concentration and their contribution to cloud condensation nuclei [3, 4]. Trees typical of boreal forests emit volatile organic compounds (VOCs), mainly monoterpenes, to the atmosphere. VOCs then undergo oxidation reactions and form low-volatility vapors, which include recently discovered highly oxygenated organic molecules (HOM) [5, 6]. They are able to condense onto tiny aerosol particles as well as directly participate in molecular clustering, thus making an important contribution to new particle formation (NPF) [5, 7].

Previous comprehensive studies [2, 8] reported the occurrence of frequent NPF in the European boreal forest environment, except for the northern edge of the area. Especially in spring, 40%–60% of days display NPF, and in many cases, these NPF events are influenced by the abundance of sulfuric acid and oxygenated organics [2, 9]. In contrast, the few studies focusing on Siberian boreal forests indicate a lower frequency of NPF events [10–13] (20%–25% West Siberia, 4%–15% Central Siberia in spring) due to unknown reasons. Determining the physical and chemical characteristics of NPF in different environments is crucial for understanding how various biogenic and anthropogenic processes affect the production of cloud condensation nuclei. In that regard,

the vast Siberian forest environment remains one of the most understudied regions.

To uncover the factors controlling the NPF frequency in the Siberian boreal forest, we investigated NPF event characteristics during spring 2020 at the Fonovaya continental background observatory. The station is surrounded by mixed forests, with agricultural and industrial centers of Russia and Kazakhstan to the south and vast wetlands and forests to the north (supplementary, figures S1(a)–(d)). The closest city of Tomsk is 60 km away. At the station, we deployed state-of-the-art instrumentation to determine the dynamics of charged and neutral clusters and particles starting from 1 nm in diameter and the composition of naturally charged molecular clusters. These measurements were supplemented by a dataset of meteorological parameters and trace gases available at the station. We analyzed clear NPF event days with *in-situ* cluster formation and particle growth, and non-event days when no change in nucleation-mode particle concentration was observed.

2. Methods

The measurements were conducted in spring 2020 (March–May) at the Fonovaya observatory, located at 56°25′ N 84°04′ E in the southeast of the West Siberian plain (supplementary, figure S1). The detailed description of the site, its climate and atmospheric circulation patterns is given in supplementary: S1.1.

The composition of charged molecules and clusters was measured using atmospheric pressure interface time-of-flight mass spectrometer, APi-TOF [14]. Particle number size distribution was derived from nano condensation nucleus counter (nCNC, 1.6–2.7 nm) [15], neutral air ion spectrometer (NAIS, 2–40 nm) [16], differential mobility particle sizer (DMPS, 6–800 nm) [17], diffusional particle sizer (DPS, 3–200 nm) [18], and optical particle counter (OPC, 0.3–20 μm) [19]. The size distribution of charged particles within 0.8–40 nm was also monitored with NAIS. The detailed description of the instrument operation as well as methods for calculation of particle formation rates (J), growth rates (GR), condensation sink (CS) and survival probability can be found in supplementary: S1 Methods.

NPF events were classified based on the particle and ion size distributions measured by NAIS and confirmed by nCNC data, see supplementary: S1.3.1. Only events with apparent particle growth, i.e., class I events [20], were taken into account. The time that separated early and late spring was defined based on the abundance of the sulfuric acid–ammonia clusters versus the abundance of clusters containing organics on NPF days as measured by APi-TOF. Early spring roughly covered a period from the onset of above-zero daily mean temperatures (beginning of March in 2020) to snowmelt; late spring — a period from snowmelt to the end of May. Sulfuric acid proxy was constructed as in [21] based on the measurements conducted at the same site with the chemical ionization APi-TOF (supplementary: S1.3.8).

Air mass back trajectories spanning 96 h and arriving at 100 m a.g.l. were calculated using HYSPLIT model [22] with 1 h resolution. We divided air mass back trajectories into ones passing over the clean sector to the north and ones passing over the dirty sector to the south of the observatory (supplementary: S1.4.2, figure S1e). Photosynthetic acclimation parameter S_{200} was calculated as in [23] (supplementary: S1.4.4).

All figures display local times, which is UTC + 07 all year. The amount of datapoints used for calculating medians in the figures is shown in tables S1 and S6. Details about the measurement site, instrumentation and calculation of different parameters can be found in supplementary material along with discussion on APi-TOF data interpretation and temperature dynamics as well as supplementary figures and tables that are referenced in the main text.

3. Results and discussion

3.1. Frequency of NPF

We were surprised to observe that NPF at the observatory Fonovaya in the spring 2020 occurred more frequently than reported in the literature [12, 13]. The onset of the NPF season was the beginning of March, similar to the other years and the other Northern Hemisphere sites [2]. Before March, we detected only one NPF event in January and one in February. In March and April, NPF events occurred on 50% and 35% of days, respectively (figure 1(a) and S2). This is about two times higher than the NPF frequency during March–April 2016–2018 at the same site when also weaker NPF events were accounted for [24]. Between 20 and 30 April 2020, no NPF was detected and the air was affected by particle emissions from wild and agricultural fires as close as 5–10 km to the measurement site. In May, after the fires, we detected a lower NPF frequency of about 15% of all days, comparable to the May-June NPF statistics of the previous years [24]. Overall, during the spring 2020, NPF events were observed on 31 days. Thus, the frequency of NPF was unusually high, in contrast to the hypothesis that NPF in Siberia is rare.

3.2. Insights into particle precursor vapors

As revealed by an APi-TOF mass spectrometer, the charged molecular cluster composition indicated a simultaneous presence of sulfuric acid, ammonia, and oxidized organics at the onset of NPF. However, the clusters' exact composition and distribution differed between periods before and after mid-April. Based on this, we separated spring 2020 into two periods: early

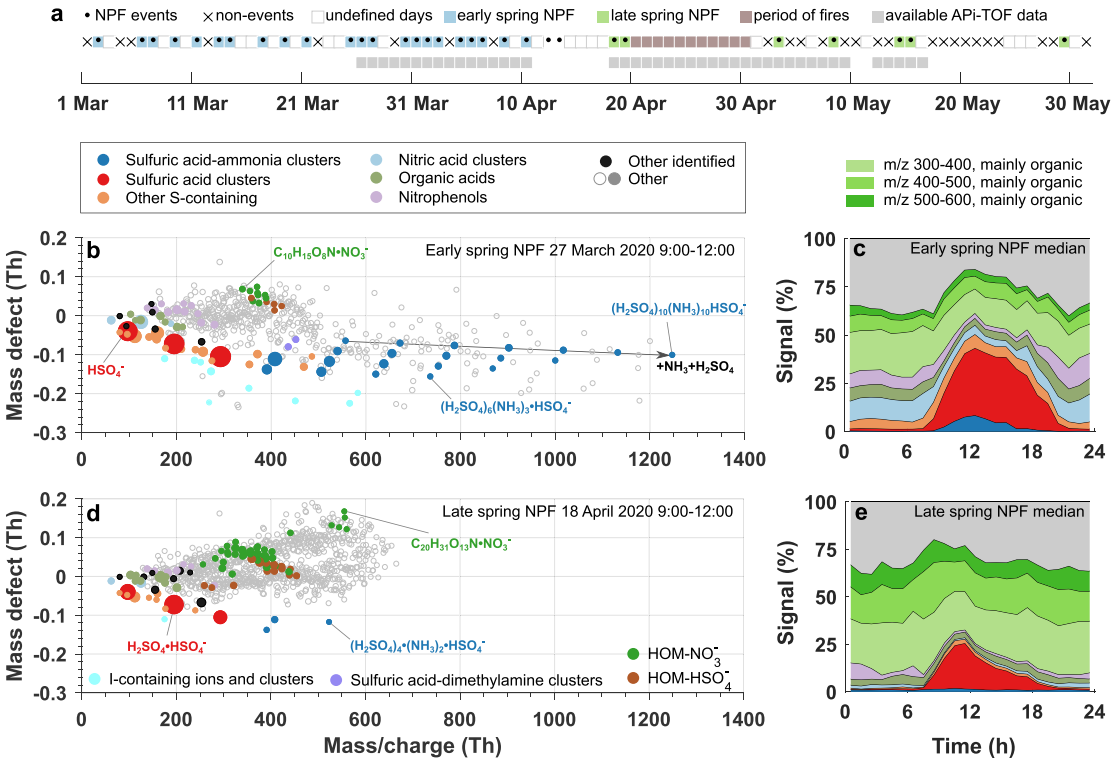

Figure 1. Chemical composition of negative ions and clusters. (a) Classification of the campaign period into NPF events, non-events and undefined days. The boundary between early spring NPF events (blue) and late spring events (green) was determined based on negative ion and molecular cluster composition as measured by APi-TOF. The days with available APi-TOF data are shown in grey. Panels (b) and (d) show mass defect as a function of mass-to-charge ratio of characteristic charged ions and molecular clusters on NPF event days during early (27 March 2020, 9:00–12:00) and late (18 April 2020, 9:00–12:00) spring, respectively. Each circle represents an ion with unique chemical composition. The size of the circles represents linearly scaled fraction of the total signal. The fraction of sulfuric acid dimer at 195 Th is approximately 10%. Note, sulfuric acid tetramer cluster is marked as sulfuric acid-ammonia cluster (see supplementary: S1 Methods). The arrow in panel (b) shows the slope of addition of 1 ammonia and 1 sulfuric acid molecule, for reference. Panels (c) and (e) depict the median contribution of different compound classes to the total signal for early ((c), $n = 11$) and late ((e), $n = 6$) spring NPF events. For panels (b)–(e), common legend is shown in a box, while other legend points are unique to either (b)/(d) or (c)/(e) panels. In comparison to panels (b) and (d), panels (c) and (e) do not show some of the compound groups due to their small fractions (see tables S2 and S3 for details), while highly oxygenated organic molecules (HOM) are more generally presented as a sum of ions in different mass-to-charge bins.

and late spring (figure 1(a)). The mass defect plots in figures 1(b) and (c) depict a snapshot of cluster composition at the onset of NPF on two specific days, while figures 1(d) and (e) show the median diel evolution of the signal for each cluster group during the early and late spring, respectively. In the early spring, a large fraction of the signal was due to sulfuric acid, sulfuric acid–ammonia, and other sulfur-containing clusters (figure 1(b)). In contrast, in late spring, we observed abundant clusters containing HOM, while the contribution of clusters containing sulfuric acid and ammonia was lower (figure 1(c)).

In early spring, the influence of anthropogenic emissions on NPF was evident. The sulfur dioxide (SO_2) concentration on the NPF days reached as high as 10 ppbv with a median daytime peak of 1.5 ppbv, higher than 0.8 ppbv on non-event days (figures S2 and S3). Using air mass trajectories, we traced the SO_2 sources to the cities and industrial areas south and southwest of the station (figures S1(c) and (d); supplementary: S1 Methods). SO_2 emissions from local or nearby sources like heating or biomass burning were also likely, though not resolved in the analysis. Higher SO_2 concentrations resulted in higher concentrations of sulfuric acid, H_2SO_4 (figure S3), which is known to initiate NPF. As sulfuric acid alone cannot efficiently form clusters at typical near-ground concentrations and temperatures, the participation of other vapors is required.

The abundance of clusters containing both sulfuric acid and ammonia on NPF days in the early spring (10% of the signal, figure 1(c)) suggested that ammonia likely contributed to molecular clustering at this site. Similar clusters were found during sulfuric acid–ammonia initiated NPF in chamber studies, in the Finnish boreal forest, over mountains, and in polar regions [25–27]. At Fonovaya, we could follow these clusters' sequential growth from a single sulfuric acid molecule to a cluster containing 11 sulfuric acid and 10 ammonia molecules (figures 1(b) and S4) further supporting that initial clustering involves these vapors. On non-event days, sulfuric acid–ammonia clusters were smaller and constituted less than 1% of the signal (figure S7(a)). The ammonia concentration during early spring was about 10–100 ppt (figure S5), which was enough to stabilize otherwise

unstable sulfuric acid clusters at atmospheric concentrations of H_2SO_4 [28]. Sources of ammonia during the early spring when the ground is covered by snow are unclear but could include nearby animal farms [29] or industrial emissions [30].

In addition, in early spring, we observed sulfuric acid clustered with other sulfur species, nitric acid, dimethylamine, iodic acid, and organics (figure 1(b), see table S2 for the exact composition). Some of these molecules are known to participate in NPF [31, 32]. Among organics, we could identify nitrophenols, which are common markers for biomass burning [33] and small organic acids (mainly carboxylic), which are not expected to participate in first steps of NPF due to their semi-volatile nature. Furthermore, we observed clusters within 200 and 500 mass-to-charge (m/z) ratios and mass defect of −0.05 and 0.1 (figure 1(b)). The ions detected within these ranges in the boreal forest correspond to HOM clusters [9]. Especially ions larger than 300 m/z can be usually classified as oxidation products of biogenic VOCs (though some small contribution of aromatic HOM to that range cannot be excluded) and are known to participate directly in molecular clustering and growth [7, 9]. Despite low signals of these clusters, we could identify few clusters as HOM, with composition consistent with the oxidation product of naturally emitted monoterpenes. These results demonstrate the influence of diverse anthropogenic and biogenic sources of vapors on NPF at Fonovaya station.

Compared to early spring, in late spring, an increase of clusters with organic material during the day is consistent with the expected increase in biogenic VOC emissions as the temperature and solar radiation increased [34–36]. During NPF events in late spring, we could identify a larger set of HOM clustered with charged sulfuric and nitric acids, similar to those observed in the Finnish boreal forest [37, 38]. In contrast, the decrease in many sulfur-containing clusters (figure 1(d) and (e)) was due to the decreases in SO_2 and sulfuric acid concentrations (figure S3). However, pure sulfuric acid clusters were still abundant, and the median sulfuric acid concentration during NPF exceeded 2×10^6 cm^{-3} (figure S3). At the same time, the fraction of the signal attributed to sulfuric acid–ammonia clusters was less than 1% compared to 10% in early spring, despite a dramatic increase in ammonia concentration after the snowmelt [39], reaching 10−30 ppb in May (figure S5). The difference between the two spring periods is likely because HOM compete with ammonia for clustering with sulfuric acid, while higher temperatures make sulfuric acid–ammonia clusters less stable and prone to easier evaporation [40]. The clusters containing oxidized organics were larger in late spring, which can be seen from the increase in the fraction of the signal attributed to ions within the 300−600 m/z range (figures 1(d) and (e)). Of these clusters, the 300−400 m/z range, similarly to early spring, could be explained by HOM monomers formed in monoterpene oxidation [5, 37, 38]. The 400−500 m/z and 500−600 m/z ranges were likely due to oxidation products of sesquiterpenes (another class of naturally emitted organics) and monoterpene HOM dimers (figure S6). Monoterpene-derived HOM dimers have very low volatility and are able to directly participate in NPF in the system containing sulfuric acid and ammonia [9]. The higher temperature in late spring promoted formation of HOM due to increased VOC emissions and rates of relevant reactions [41], but also likely caused an increase in HOM volatility making them less efficient at forming clusters and particles than in early spring.

Based on existing knowledge of NPF in boreal forest [9], it is plausible to hypothesize that at observatory Fonovaya, all three components (sulfuric acid, ammonia and biogenic HOM) play important role in NPF during both spring periods. The relative importance of each component, however, is controlled by temperature and availability of vapor molecules. It is important to note that without additional measurements, we cannot fully exclude that other vapors, such as amines, participate in clustering.

3.3. Particle formation and growth rates

In early spring, NPF events were usually strong and intensive but in late spring, they were weak with intermittent particles' growth (figure S2). This was reflected both in number concentrations of 3−30 nm particles measured by the NAIS and in the sub-3 nm cluster and particle concentrations derived from the nCNC (figure 2(a)). Clear peaks in the number concentrations were observed in all the size bins in the 1.3−30 nm diameter range on the NPF event days. Oppositely, the corresponding concentrations on non-event days were flat and low (figure S7). The peak number concentrations in the 3−30 nm range were 5−10 times higher during the median early spring NPF event compared to the median late spring NPF event. At the same time, during NPF events in late spring (figure 2(b)), the number concentrations of clusters and particles in the size bins of 1.3−1.6 nm, 1.6−2.1 nm and 3−6 nm closely matched those measured at the Finnish station SMEAR II [42, 43]. Thus, the median Siberian NPF event in early spring was stronger than the median one at SMEAR II as 5−10 times more particles were formed.

In agreement with cluster and particle number concentrations, the median total particle formation rates of 3-nm particles ($J_{3\ tot}$) were higher in early spring than in late spring (table S1), 2.2 and 0.4 cm^{-3} s^{-1}, respectively. In addition, the growth rates of 2−3 nm particles were also higher: 1.7 nm h^{-1}

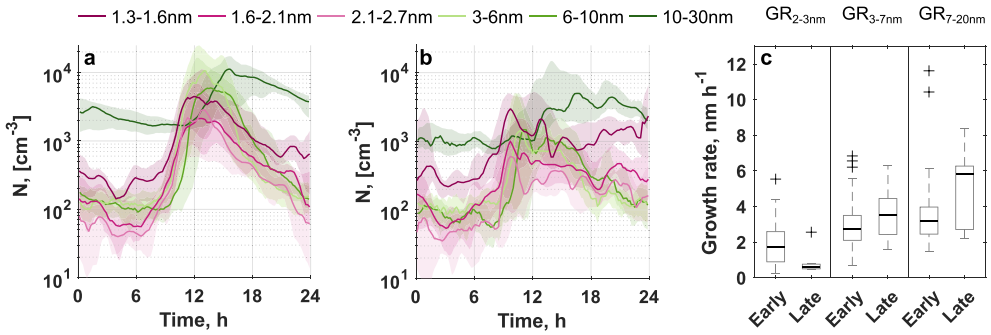

Figure 2. Median particle number concentrations and growth rates. Median particle number concentrations in different size bins measured on NPF days during (a) early spring ($n = 22$) and (b) late spring ($n = 7$). Particles within 1.3−2.7 nm are measured by nCNC (pink) and particles 3−30 nm are measured by NAIS in neutral particle mode (green). Solid lines are medians with 25th to 75th percentiles represented as shaded areas. (c) Particle growth rates (GR) in different size bins for early and late spring. Median values are marked in black solid line, box edges represent 25th and 75th percentiles, whiskers show $\pm 2.7\sigma$, and outliers are shown as plus markers (for n, see table S1). The difference between the median values of growth rates in early and late spring is statistically significant only for GR_{2-3} ($p = 0.04$, Wilcoxon rank sum test).

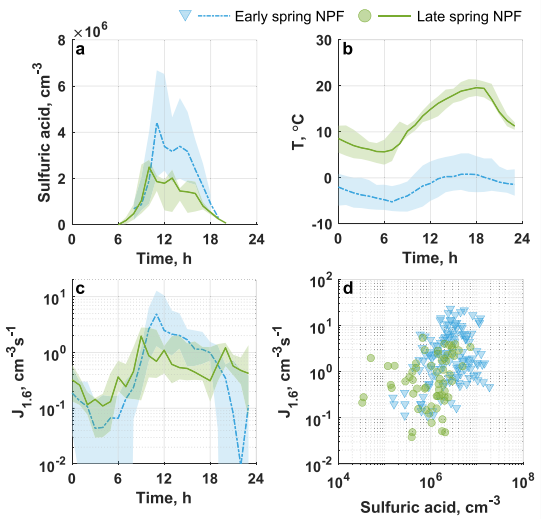

Figure 3. Sulfuric acid, temperature, and particle formation rates. Median diel evolution of sulfuric acid ($n = 19$ and 7) (a), temperature ($n = 22$ and 7) (b) and particle formation rates at 1.6 nm $J_{1.6}$ ($n = 20$ and 7) (c). Solid lines show medians with shaded areas representing 25th to 75th percentiles. Panel (d) depicts $J_{1.6}$ as a function of sulfuric acid concentration. Early spring is characterized by higher sulfuric acid concentration and lower temperature resulting in higher particle formation rates than in late spring.

in early spring in comparison to 0.6 nm h^{-1} in late spring (figure 2(c)). Oppositely, the median growth rates of bigger particles were higher in late spring (2.7 vs. 3.5 nm h^{-1} and 3.2 vs. 5.8 nm h^{-1} for particles in size ranges of 3−7 nm and 7−20 nm, respectively); however, the difference was not statistically significant. The larger growth rates of 2−3 nm particles during early spring are consistent with the higher concentrations of non-volatile sulfuric acid and lower temperatures during that period (figures 3(a), (b) and S3).

The neutral pathway dominated particle formation during both early and late spring events. This is confirmed by the larger number concentration of neutral particles within 2–3 nm as compared to that of ions, about 1–2 orders of magnitude (figure S8). In addition, similarly to many other sites [45], formation rates of charged particles at 2 nm ($J_{2\ ion}$) were much lower than the corresponding total particle formation rate $J_{1.6\ tot}$ during both periods, with median values of 0.02–0.04 $cm^{-3}\ s^{-1}$ in comparison to 1–2 $cm^{-3}\ s^{-1}$ (table S1). $J_{1.6\ tot}$ and $J_{3\ tot}$ in late spring were around a factor of 3–4 smaller in comparison to the early spring (figure 3(c), table S1). The variability in J in the atmosphere is typically a function of precursor concentration, condensation sink, and temperature: $J_{1.6\ tot}$ exhibited a positive relationship with the calculated sulfuric acid concentration (figure 3(d)). Higher temperature which decreases cluster stability and lowers sulfuric acid concentrations (figures 3(a) and (b)) could explain lower values of $J_{1.6\ tot}$ in late spring. When comparing to laboratory parameterizations of formation rates, $J_{1.6}$ at Fonovaya were higher than those predicted for the system that includes only sulfuric acid, ammonia and water [28] during the whole spring, suggesting there is a contribution of other vapors, likely HOM, to clustering and NPF.

Overall, in early spring, we saw higher formation and growth rate of small particles, in line with the higher observed NPF frequency. The formation rate of 1.6 nm particles (figures 3(c) and (d)) is similar or somewhat higher than at other boreal forest sites [9, 42, 46]. However, larger values of condensation sink and relatively low growth rate of 2−3 nm particles result in a low survival probability of particles against coagulation scavenging in this Siberian site (figure S3). For the early and late spring, survival probabilities of particles from 2 to 3 nm were 0.26 and 0.08,

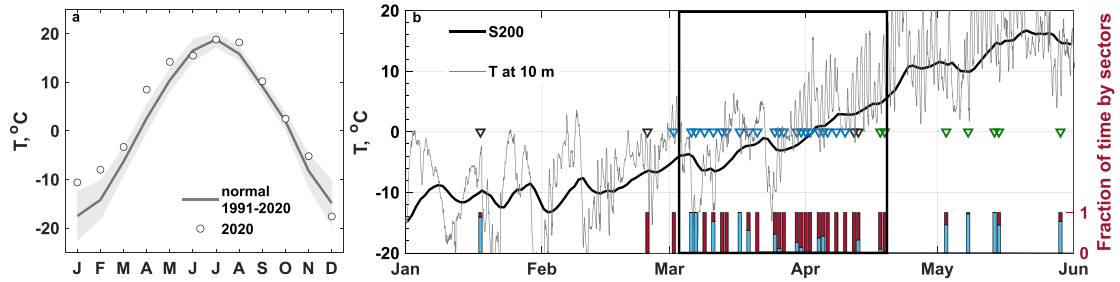

Figure 4. Temperature and airmass history during 2020. (a) Climatological normal of monthly-mean temperatures measured at the meteorological station Tomsk, 60 km to north-east from Fonovaya (www.meteo.ru, last access 5 January 2022). Solid line shows monthly mean values while shadow depicts $\pm 1\sigma$. Round symbols show monthly-mean temperatures calculated from the current data set for Fonovaya observatory for 2020. Approximately one-month shift to warmer temperatures can be seen for winter—spring 2020 as compared to the normal. (b) Time series of air temperature (gray) and S_{200} (black)—the parameter characterizing the state of photosynthetic acclimation (supplementary: S1 methods). The rectangular area marks the period when the photosynthetic efficiency increases from 0% to 50% of its summer maximum ($-4\,°C < S_{200} < 6\,°C$) [44] and when monoterpene emissions bursts were observed in a boreal forest in Finland [23]. NPF days are shown by symbols: blue—early spring NPF days, green—late spring NPF days, black—unclassified NPF (figure 1(a)). The bar plot shows the median fraction of daytime when an air mass trajectory was in the clean (light blue) or dirty (dark red) sector (within the mixed layer).

respectively, compared to 0.83 in the Finnish boreal forest [47]. The importance of particle survival from 2 to 3 nm for NPF is also evident from figure S7: on non-event days, especially in late spring, concentrations of the smallest particles (1.3−1.6 nm and 1.6−2.1 nm) remain relatively high at a few hundred cm^{-3}, whereas concentrations of 2.1−2.7 nm particles are low at few tens cm^{-3}.

3.4. The effect of meteorology on NPF

To understand the onset of frequent NPF in the early spring and the change in NPF characteristics in mid-April, we looked in more detail at meteorological conditions. Siberia experienced a heatwave that lasted almost half a year in winter-spring 2020 ([48], supplementary: S2.2). A comparison with typical monthly mean temperatures shows that the spring came about one month earlier (figure 4(a)) and the start of photosynthesis in March (figure 4(b)) coincided with the series of intense NPF events. This finding and the almost complete absence of NPF in winter suggest that organic compounds emitted from forests play an essential role in NPF even when sulfuric acid and sulfuric acid–ammonia clusters dominate the charged cluster composition. Even though observed HOM clusters were less abundant in early than late spring, lower temperature could explain the observed particle formation rates (figure 3 and supplementary: S1.3.9).

The air mass transfer at the station is dominated by a semi-permanent large-scale anticyclone — the Siberian high (supplementary: S1 Methods) and follows the same pattern from year to year. It develops in October and persists approximately till the end of April. In winter, the Siberian high induces a south-westerly airflow, but after its dissipation in April, the predominant direction of an atmospheric flow becomes north-westerly. In agreement with this description, a large fraction of air masses during early spring came from industrial and agricultural sources south and southwest, bringing anthropogenic SO_2 and possibly ammonia. Particularly on the NPF days, the median time spent by the trajectories in the clean northern sector was zero (see bar plot in figures 4(b) and S9(a)). In late spring, air masses often arrived from the clean north-northwest (figures 4(b) and S9(b)) although during NPF events, they always spent some time over the pollution sources (figure S9(b)) and were likely enriched with SO_2. The low temperatures in early spring (figure 3(b)) promoted the stability of newly formed clusters. Thus, the early onset of photosynthesis and simultaneous air mass transfer from the polluted sector likely triggered strong NPF in March–April over this Siberian forest. This is in contrast to the European stations, where strong NPF are typically observed in connection with air masses from the clean sector [46, 49].

In agreement with our hypothesis above, during the last five years a warmer March had two times as many NPF events as a mean or cold March (figure S10(b)). NPF frequency in a warmer March was similar to that at SMEAR II in Finland (40%–60%). The detailed trends of monthly mean temperatures (figures S10(c)–(f)) showed that February and March are warming faster than other months, at the rate of 1 °C/decade. With this warming rate and a current monthly mean March temperature of −5 °C (figure S10(c)), the temperature of −2.5…−2 °C favoring a higher NPF frequency (figure S10(b)) will be reached already within the next 25−30 years.

4. Conclusion

Our results suggest that interactions between anthropogenic and biogenic vapors drive NPF at the forest

site in West Siberia, and the same is likely seen along the southern forest edge of the region. For the first time, we show the measurements of particle precursor vapors in Siberia. Sulfuric acid, ammonia, and biogenic organic vapors play a role in both early and late spring NPF events, but with different contributions. As temperature increases towards summer, there are more organics that undergo oxidation faster. However, at the same time, clusters are less stable, and vapors are more volatile, causing NPF to be weaker. In agreement with this, in late spring the probability of particle survival during their growth from 2 to 3 nm is below 10% due to low growth rate and relatively high condensation sink.

We hypothesize that early spring with warmer temperatures triggered biogenic activity, which caused a high NPF frequency in air masses from polluted areas. Thus, in a warmer climate, West Siberian forests have the potential to become at least two times stronger aerosol sources in early spring compared with the present, with NPF frequencies observed currently in the Finnish boreal forest. However, in the long-term perspective, variability of atmospheric circulation patterns should be considered. Based on the suggested link between meteorological processes and NPF frequency, we identify future research directions of Siberian NPF with a focus on anthropogenic and biogenic VOC measurements. Moreover, our data set opens new possibilities for benchmarking of atmospheric and chemical transfer models. Verified models can then be used to study NPF dynamics in time and space, and further advance our understanding of the impact of Siberian NPF on climate.

It is important to note that in Siberian taiga we observe frequent NPF in anthropogenically influenced, 'dirty' air masses in contrast to the Finnish boreal forest where NPF occurs in the air masses from the clean sector. While the chemical mechanisms of NPF in boreal forest is consistent across measured locations so far, the combination of external parameters that provide favorable conditions for NPF differ. We, therefore, emphasize the heterogeneity of the boreal forest environment and call for long term measurements of aerosol particles and their precursors in other locations around the world.

Data availability statement

The data that support the findings of this study are openly available at the following URL/DOI: https://zenodo.org/doi/10.5281/zenodo.10211385.

Acknowledgments

We acknowledge the following Projects: ACCC (The Atmosphere and Climate Competence Center) Flagship funded by the Academy of Finland Grant No. 337549, Academy professorship funded by the Academy of Finland (Grant No. 302958), Belmont Forum project funded by Academy of Finland Grant No. 334792, Academy of Finland Project Nos. 325656, 316114 and 325647, Academy of Finland mobility Grant Nos. 333581, 334625, 'Quantifying carbon sink, CarbonSink+ and their interaction with air quality' INAR Project funded by Jane and Aatos Erkko Foundation, European Research Council (ERC) Project ATM-GTP (Atmospheric Gas-to-Particle conversion) Contract No. 742206, CHAPAs Grant No. 850614 and ADAPT (Autoxidation of Anthropogenic Volatile Organic Compounds (AVOC) as a Source of Urban Air Pollution) Grant No. 101002728, Russian Foundation for Basic Research Project No. 19-05-50024, Ministry of Education and Science of the Russian Federation Grant No. 075-15-2021-934, EMME-CARE (The Eastern Mediterranean and Middle East—Climate and Atmosphere Research) Project which received funding from the European Union's Horizon 2020 Research and Innovation Programme, under Grant Agreement No. 856612 and from the Cyprus Government. O G received funding from Doctoral Programme in Atmospheric Sciences at the University of Helsinki. Help with instrument preparation, codes and troubleshooting from J Lampilahti, M Lampimäki, P Aalto, T Laitinen, P Rantala, F Korhonen, E Siivola, J Mäntylä, H Koskenvaara, P Keronen, L Dada, E Nikitina, M Ehn, H Junninen, C Yan is gratefully acknowledged. We thank tofTools team for proving tools for mass spectrometry data analysis. The authors gratefully acknowledge the NOAA Air Resources Laboratory (ARL) for the provision of the HYSPLIT transport and dispersion model.

Author contributions

M K, T P, B B, O G and E E conceived the study. O G, E E, T P, M A, D D, B B and M K organized the measurement campaign. O G, M A, D D and A L conducted field measurements. O G, E E, A L, M R, D A analyzed data. V M K, M K, T P, M A, B B, F B, R B, T C contributed to scientific discussion. O G and E E interpreted the results and wrote the manuscript with the help of the co-authors.

ORCID iDs

Olga Garmash https://orcid.org/0000-0002-9675-3271
Ekaterina Ezhova https://orcid.org/0000-0003-2770-9143
Mikhail Arshinov https://orcid.org/0000-0002-4599-8287
Meri Räty https://orcid.org/0000-0001-9361-4885
Diego Aliaga https://orcid.org/0000-0001-6781-4568
Rima Baalbaki https://orcid.org/0000-0002-4480-2107

Tommy Chan https://orcid.org/0000-0002-5700-7209
Federico Bianchi https://orcid.org/0000-0003-2996-3604
Veli-Matti Kerminen https://orcid.org/0000-0002-0706-669X
Tuukka Petäjä https://orcid.org/0000-0002-1881-9044
Markku Kulmala https://orcid.org/0000-0003-3464-7825

References

[1] Tunved P, Hansson H-C, Kerminen V-M, Ström J, Maso M D, Lihavainen H, Viisanen Y, Aalto P P, Komppula M and Kulmala M 2006 High natural aerosol loading over boreal forests *Science* **312** 261–3
[2] Kerminen V-M, Chen X, Vakkari V, Petäjä T, Kulmala M and Bianchi F 2018 Atmospheric new particle formation and growth: review of field observations *Environ. Res. Lett.* **13** 103003
[3] Merikanto J, Spracklen D V, Mann G W, Pickering S J and Carslaw K S 2009 Impact of nucleation on global CCN *Atmos. Chem. Phys.* **9** 8601–16
[4] Spracklen D V, Bonn B and Carslaw K S 2008 Boreal forests, aerosols and the impacts on clouds and climate *Phil. Trans. R. Soc.* A **366** 4613–26
[5] Ehn M *et al* 2014 A large source of low-volatility secondary organic aerosol *Nature* **506** 476–9
[6] Bianchi F *et al* 2019 Highly oxygenated organic molecules (HOM) from gas-phase autoxidation involving peroxy radicals: a key contributor to atmospheric aerosol *Chem. Rev.* **119** 3472–509
[7] Kirkby J *et al* 2016 Ion-induced nucleation of pure biogenic particles *Nature* **533** 521–6
[8] Nieminen T *et al* 2018 Global analysis of continental boundary layer new particle formation based on long-term measurements *Atmos. Chem. Phys.* **18** 14737–56
[9] Lehtipalo K *et al* 2018 Multicomponent new particle formation from sulfuric acid, ammonia, and biogenic vapors *Sci. Adv.* **4** eaau5363
[10] Heintzenberg J, Birmili W, Otto R, Andreae M O, Mayer J-C, Chi X and Panov A 2011 Aerosol particle number size distributions and particulate light absorption at the ZOTTO tall tower (Siberia), 2006–2009 *Atmos. Chem. Phys.* **11** 8703–19
[11] Chi X, Winderlich J, Mayer J-C, Panov A V, Heimann M, Birmili W, Heintzenberg J, Cheng Y and Andreae M O 2013 Long-term measurements of aerosol and carbon monoxide at the ZOTTO tall tower to characterize polluted and pristine air in the Siberian taiga *Atmos. Chem. Phys.* **13** 12271–98
[12] Dal Maso M *et al* 2008 Aerosol particle formation events at two Siberian stations inside the boreal forest *Boreal Environ. Res.* **13** 81–92
[13] Uusitalo H *et al* 2021 Occurrence of new particle formation events in Siberian and Finnish boreal forest *Atmos. Chem. Phys. Discuss.* 1–21
[14] Junninen H *et al* 2010 A high-resolution mass spectrometer to measure atmospheric ion composition *Atmos. Meas. Tech.* **3** 1039–53
[15] Vanhanen J, Mikkilä J, Lehtipalo K, Sipilä M, Manninen H E, Siivola E, Petäjä T and Kulmala M 2011 Particle size magnifier for nano-CN detection *Aerosol Sci. Technol.* **45** 533–42
[16] Manninen H E, Mirme S, Mirme A, Petäjä T and Kulmala M 2016 How to reliably detect molecular clusters and nucleation mode particles with neutral cluster and air ion spectrometer (NAIS) *Atmos. Meas. Tech.* **9** 3577–605
[17] Aalto P *et al* 2001 Physical characterization of aerosol particles during nucleation events *Tellus* B **53** 344–58
[18] Reischl G P, Majerowicz A, Ankilow A, Eremenko S and Mavliev R 1991 Comparison of the novosibirsk automated diffusion battery with the vienna electro mobility spectrometer *J. Aerosol Sci.* **22** 223–8
[19] Sousan S, Koehler K, Hallett L and Peters T M 2016 Evaluation of the Alphasense optical particle counter (OPC-N2) and the Grimm portable aerosol spectrometer (PAS-1.108) *Aerosol Sci. Technol.* **50** 1352–65
[20] Dal Maso M *et al* 2005 Formation and growth of fresh atmospheric aerosols: eight years of aerosol size distribution data from SMEAR II, Hyytiälä, Finland *Boreal Environ. Res.* **10** 323–36 (available at: www.borenv.net/BER/archive/pdfs/ber10/ber10-323.pdf)
[21] Petäjä T, Mauldin, III R L, Kosciuch E, McGrath J, Nieminen T, Paasonen P, Boy M, Adamov A, Kotiaho T and Kulmala M 2009 Sulfuric acid and OH concentrations in a boreal forest site *Atmos. Chem. Phys.* **9** 7435–48
[22] Stein A F, Draxler R R, Rolph G D, Stunder B J B, Cohen M D and Ngan F 2015 NOAA's HYSPLIT atmospheric transport and dispersion modeling system *Bull. Am. Meteorol. Soc.* **96** 2059–77
[23] Aalto J, Porcar-Castell A, Atherton J, Kolari P, Pohja T, Hari P, Nikinmaa E, Petäjä T and Bäck J 2015 Onset of photosynthesis in spring speeds up monoterpene synthesis and leads to emission bursts *Plant Cell Environ.* **38** 2299–312
[24] Lampilahti A *et al* 2023 New particle formation in boreal forests of Siberia, Finland and Estonia *Boreal Environ. Res.* **28** 147–67 (available at: www.borenv.net/BER/archive/pdfs/ber28/ber28-147-167.pdf)
[25] Schobesberger S *et al* 2015 On the composition of ammonia–sulfuric-acid ion clusters during aerosol particle formation *Atmos. Chem. Phys.* **15** 55–78
[26] Frege C *et al* 2017 Chemical characterization of atmospheric ions at the high altitude research station Jungfraujoch (Switzerland) *Atmos. Chem. Phys.* **17** 2613–29
[27] Beck L J *et al* 2021 Differing mechanisms of new particle formation at two arctic sites *Geophys. Res. Lett.* **48** e2020GL091334
[28] Kürten A *et al* 2016 Experimental particle formation rates spanning tropospheric sulfuric acid and ammonia abundances, ion production rates, and temperatures *J. Geophys. Res.* **121** 12377–400
[29] Sapozhnikov P M, Granina N I and Kulizhskii S P 2021 Comparative characteristics of the cadastral value of agrolandscapes of the Siberian Federal District (as exemplified by Irkutsk and Tomsk oblasts) *IOP Conf. Ser.: Earth Environ. Sci.* **862** 012010
[30] Van Damme M, Clarisse L, Whitburn S, Hadji-Lazaro J, Hurtmans D, Clerbaux C and Coheur P-F 2018 Industrial and agricultural ammonia point sources exposed *Nature* **564** 99–103
[31] Yao L *et al* 2018 Atmospheric new particle formation from sulfuric acid and amines in a Chinese megacity *Science* **361** 278–81
[32] Sipilä M *et al* 2016 Molecular-scale evidence of aerosol particle formation via sequential addition of HIO_3 *Nature* **537** 532–4
[33] Harrison M A J, Barra S, Borghesi D, Vione D, Arsene C and Iulian Olariu R 2005 Nitrated phenols in the atmosphere: a review *Atmos. Environ.* **39** 231–48
[34] Tingey D T, Manning M, Grothaus L C and Burns W F 1980 Influence of light and temperature on monoterpene emission rates from slash pine *Plant Physiol.* **65** 797–801
[35] Monson R K, Jaeger C H, Adams W W, Driggers E M, Silver G M and Fall R 1992 Relationships among isoprene emission rate, photosynthesis, and isoprene synthase activity as influenced by temperature 1 *Plant Physiol.* **98** 1175–80
[36] Lappalainen H K, Sevanto S, Bäck J, Ruuskanen T M, Kolari P, Taipale R, Rinne J, Kulmala M and Hari P 2009 Day-time concentrations of biogenic volatile organic compounds in a boreal forest canopy and their relation to environmental and biological factors *Atmos. Chem. Phys.* **9** 5447–59

[37] Ehn M et al 2012 Gas phase formation of extremely oxidized pinene reaction products in chamber and ambient air Atmos. Chem. Phys. 12 5113–27
[38] Bianchi F et al 2017 The role of highly oxygenated molecules (HOMs) in determining the composition of ambient ions in the boreal forest Atmos. Chem. Phys. 17 13819–31
[39] Flesch T K, Baron V S, Wilson J D, Griffith D W T, Basarab J A and Carlson P J 2016 Agricultural gas emissions during the spring thaw: applying a new measurement technique Agric. For. Meteorol. 221 111–21
[40] Yan C et al 2018 The role of H_2SO_4-NH_3 anion clusters in ion-induced aerosol nucleation mechanisms in the boreal forest Atmos. Chem. Phys. 18 13231–43
[41] Quéléver L L J et al 2019 Effect of temperature on the formation of highly oxygenated organic molecules (HOMs) from alpha-pinene ozonolysis Atmos. Chem. Phys. 19 7609–25
[42] Kulmala M et al 2013 Direct observations of atmospheric aerosol nucleation Science 339 943–6
[43] Kulmala M et al 2022 Towards a concentration closure of sub-6 nm aerosol particles and sub-3 nm atmospheric clusters J. Aerosol Sci. 159 105878
[44] Kolari P, Lappalainen H K, Hänninen H and Hari P 2007 Relationship between temperature and the seasonal course of photosynthesis in Scots pine at northern timberline and in southern boreal zone Tellus B 59 542–52
[45] Manninen H E et al 2010 EUCAARI ion spectrometer measurements at 12 European sites—analysis of new particle formation events Atmos. Chem. Phys. 10 7907–27
[46] Vana M et al 2016 Characteristics of new-particle formation at three SMEAR stations Boreal Environ. Res. 21 345–62 (available at: www.borenv.net/BER/archive/pdfs/ber14/ber14-683.pdf)
[47] Kulmala M, Kerminen V-M, Petäjä T, Ding A J and Wang L 2017 Atmospheric gas-to-particle conversion: why NPF events are observed in megacities? Faraday Discuss. 200 271–88
[48] Overland J E and Wang M 2021 The 2020 Siberian heat wave Int. J. Climatol. 41 E2341–6
[49] Sogacheva L, Saukkonen L, Nilsson E D, Dal Maso M, Schultz D M, De Leeuw G and Kulmala M 2008 New aerosol particle formation in different synoptic situations at Hyytiälä, Southern Finland Tellus B 60 485–94